Journal of Physics: Conference Series **122** (2008) 012022 doi:10.1088/1742-6596/122/1/012022

The experimental plan of displacement- and frequency-noise free laser interferometer

K Kokeyama[1], S Sato[2], A Nishizawa[3], S Kawamura[2], Y Chen[4], RL Ward[5], A Pai[4], K Somiya[4], and A Sugamoto[6]

[1] Graduate School of Humanities and Sciences, Ochanomizu University, 2-1-1, Otsuka, Bunkyo-ku, Tokyo, 112-8610 Japan
[2] TAMA Project, National Astronomical Observatory of Japan, 2-21-1, Osawa, Mitaka, Tokyo 181-8588 Japan
[3] Graduate School of Human and Environmental Studies, Kyoto University, Kyoto 606-8501, Japan
[4] Max-Planck-Institut für Gravitationsphysik, Am Mühlenberg 1, 14476 Potsdam, Germany
[5] LIGO Project 18-34, California Institute of Technology, Pasadena, California 91125, USA
[6] Ochanomizu University, 2-1-1, Otsuka, Bunkyo-ku, Tokyo, 112-8610 Japan

E-mail: keiko.kokeyama@nao.ac.jp

Abstract. We present the partial demonstration of displacement- and laser-noise free interferometer (DFI) and the next experimental plan to examine the complete configuration. A part of the full implementation of DFI has been demonstrated to confirm the cancellation of beamsplitter displacements. The displacements were suppressed by about two orders of magnitude. The aim of the next experiment is to operate the system and to confirm the cancellation of all displacement noises, while the gravitational wave (GW) signals survive. The optical displacements will be simulated by electro-optic modulators (EOM). To simulate the GW contribution to laser lights, we will use multiple EOMs.

1. Introduction

Gravitational waves (GW) have been searched for years by ground-based GW detectors [1-6]. However, they have not been detected yet since their amplitudes are quite tiny and the detectors are disturbed by a great amount of noise. The sensitivities of the detectors are limited by various noises, e.g., seismic- and gravity gradient disturbances, thermal noises in mirrors and suspensions, and shot noises. Recently, theoretical investigation of the GW detectors which are free from both the displacement noises of the optics and the laser frequency noises have been proposed [7, 8]. In these two papers, it was shown that when an N-test-mass array ($N > d+2, d$ is the spatial dimension of the array of test masses) consists of multiple interferometers, a signal combination which does not sense displacement- and frequency-noises but sense the GW contribution can be constructed. It is carried out by the fact that the GW contribution to phase shifts of laser light takes a form different from that of optical displacements.

In the next section, the DFI configuration suggested in [9] will be introduced. In section 3, the result of a proof-of-principle experiment will be presented. The experimental plan of the next experiment will be explained in section 4.

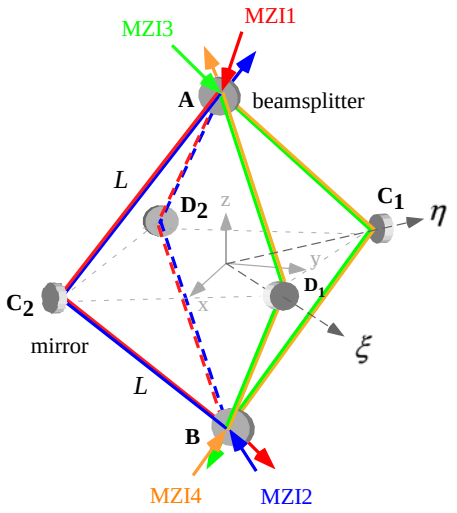

Figure 1. The 3-D DFI configuration. It consists of 4 Mach-Zehnder interferometers, MZI1, MZI2, MZI3 and MZI4. A and B are beamsplitters, and $C_{1,2}$ and $D_{1,2}$ are steering mirrors. Path lengths between mirrors and beamsplitters are L. The light path of MZI1 is $A_tD_2B_r$ - $A_rC_2B_t$; MZI2 is $B_tD_2A_r$ - $B_rC_2A_t$; MZI3 is $A_tC_1B_r$-$A_rD_1B_t$; MZI4 is $B_tC_1A_r$ -$B_rD_1A_t$;. The subscripts r and t denote reflection and transmission at the beamsplitters.

2. DFI configuration

Reference [9] proposed 2D and 3D optical designs of DFI implemented by four Mach-Zehnder interferometers (MZI). Figure 1 shows the 3D design that will be based. In this octahedron configuration, two MZIs are combined to construct one bidirectional MZI where the two MZIs are counterpropagating on the same optical path. The path length of AC_2, C_2B, AD_2, and D_2B are the same so that the MZI1 and MZI2 responses to the folding mirrors are identical. The displacements of the two folding mirrors are detected redundantly by the two MZIs and can be eliminated clearly by combining the two signals. To eliminate the beamsplitter displacements, an additional pair of identical bidirectional MZIs is employed. Thus the two pairs of bidirectional MZIs sense the two beamsplitters redundantly and the displacement noises can be removed. The frequency noises are canceled by each MZI itself because of the same arm lengths (AC_2B and AD_2B for MZI1 and MZI2, AC_1B and AD_1B for MZI3 and MZI4). The GW signals will remain in the combined signal because the GW and displacement noises contribute to light propagation in different manners. As discussed in [9], the DFI signal has the GW response which is proportional to $(\Omega_{\rm GW}L/c)^2$ for 3D configuration in the low frequency range, where $\Omega_{\rm GW}$ is the GW frequency.

3. Partial demonstration

So far, the displacement noises of the folding mirrors were simulated by EOMs and a suppression of about 45 dB was attained by using one bidirectional MZI [10]. The beamsplitter motion has also been simulated by an EOM and the suppression of the displacement noises was confirmed [11]. For the next step, we actually actuated the beamsplitter, and confirmed the cancellation of the displacement-noise signals. In this experiment, the GW effects were not simulated.

3.1. Experiment

Depicted in Fig. 2 is the optical layout of this experiment. Four mirrors and two beamsplitters compose two MZIs which share the beamsplitters. These interferometers expressed in 2D correspond to the combination of MZI1 and MZI3 in Fig. 1. In this 2D configuration, the two input beams enter the interferometer. The incident beam of MZI1 is parallel to the x axis. The incident beam of MZI3 is in the angle θ_3 ($\pi/4 < \theta_3 < 3\pi/4$) in respect to the x axis. The two beams are separated by beamsplitter A, then propagate the inline arms (AD_2B and AC_1B, for MZI1 and MZI3, respectively) and the perpendicular arms (AC_2B and AD_1B, for MZI1

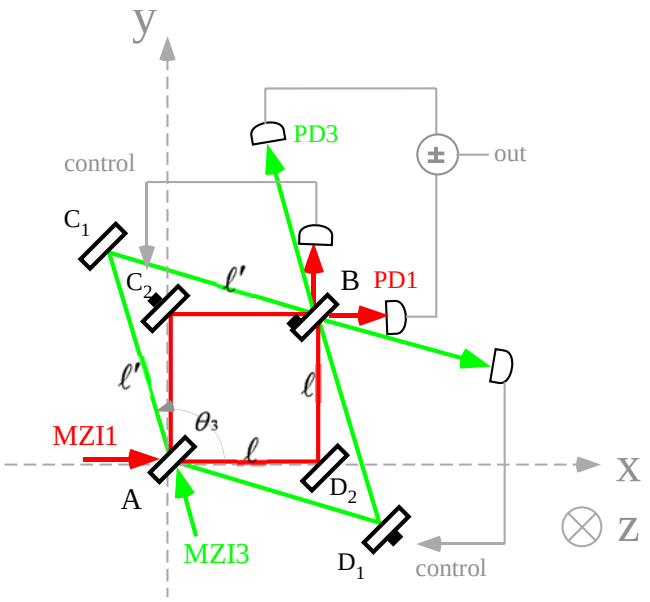

Figure 2. The setup for the proof-of-principle experiment. The two MZIs are symmetric across the AB axis. ℓ and ℓ' denote the length between a beamsplitter and a mirror of MZI1 and MZI3, respectively. The path AD_2 of MZI1 is parallel to the x axis. The path AC_1 of MZI3 is in the angle θ_3 ($\pi/4 < \theta_3 < 3\pi/4$) in respect to the x axis. The beamsplitter B are actuated by an attached PZT. This displacement is sensed by the two MZIs redundantly. The two outputs (out1 and out3 for MZI1 and MZI3) are electrically subtracted so that the beamsplitter displacement signals are suppressed.

and MZI3, respectively). Here, we defined that the inline arm is the path transmitting A and the perpendicular arm is the path reflected by A. The two beams interfere after the second beamsplitter, B. There are two output ports after the second beamsplitter. The laser fields are detected by the photo detectors, PD1 and PD3, for MZI1 and MZI3, respectively. One of the output signals is used to control via mid-fringe locking. The other signal is to monitor the beamsplitter displacements. The PZT (piezoelectric transducer) is attached to the beamsplitter-holder to simulate displacement noises. The output signals of MZI1 (out1) and MZI3 (out3) are sent to the electric subtracter to cancel the displacement noises.

When beamsplitter B is excited by the attached PZT at an angular frequency and an amplitude $d\ell_0$, the paths length are changed. The output voltages of PD1 and PD3 can be respectively written as,

$$V_{\mathrm{PD1}}(\omega) \propto \frac{\omega_0 d\ell_1}{c} \tag{1}$$

$$V_{\mathrm{PD3}}(\omega) \propto \frac{\omega_0 d\ell_3}{c} \tag{2}$$

where ω_0 is the angular frequency of the laser light. $d\ell_1 = \sqrt{2}d\ell_0$ and $d\ell_3 = \frac{1-\cos(2\theta_3)}{\cos(3\pi/4-\theta_3)}d\ell_0$ are caused by the angles of the beamsplitter. Subtracting these two signals, we can remove the displacement-noise signals. In order to the maximal subtraction, the photo intensities at the two detectors were adjusted in such a way that the two output voltages agree at the outside the control band. In addition, the control gains were adjusted so that the control ranges agree among the two MZIs.

3.2. Result

Figure 3 shows the result of the displacement-noise suppression. The plots are the magnitude and phase of the transfer functions from the actuated beamsplitter to out1, out3, and the subtracted signal, including the response functions of the PZT and the photo detectors. The magnitude of out1 and out3 were tuned appropriately so that the displacement-noise signals are maximally canceled. About two orders of suppression was achieved in a frequency region in

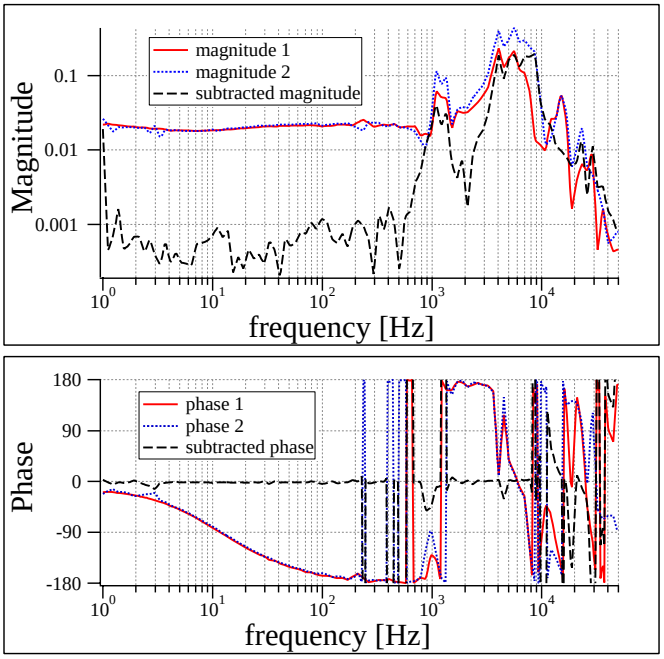

Figure 3. Magnitude and phases of the transfer function from beamsplitter displacements to output signals. Solid-red and dashed-blue plots are magnitudes of the transfer function from the beamsplitter to PD1 and PD3, respectively, giving almost same response below about 1 kHz. Dotted-black lines are magnitude and phase of the DFI signal. Approximately two orders of magnitude of suppression can be seen from DC to 1 kHz. The suppression depends on subtle adjustments of the balance between the two outputs.

which the PZT can be excited consistently. Many mechanical resonants due to the PZT, and ones caused by coupling of the PZT and the beamsplitter were seen above 1 kHZ. In this region, the displacement-noise were not canceled.

4. Experimental Plan for 3D Full Configuration

In our next experiment, the DFI will be constructed in 3D space and operated in the full configuration just as shown in Fig. 1. We will confirm that all test-mass displacements are canceled while GW signals are retained in the DFI signals. The mirror displacements, beamsplitter displacements, and the GW effects should be simulated.

The signals of the four MZIs will be extracted and combined so that displacement noises disappear. The output voltage of each interferometer can be written in frequency domain

$$V_1(\Omega) \propto \frac{\omega_0}{c}\left[dx_{C_2}e^{i\Omega L/c} + dx_{D_2}e^{i\Omega L/c} + dx_A e^{2i\Omega L/c} + dx_B\right] \tag{3}$$

$$V_2(\Omega) \propto \frac{\omega_0}{c}\left[dx_{C_2}e^{i\Omega L/c} + dx_{D_2}e^{i\Omega L/c} + dx_A + dx_B e^{2i\Omega L/c}\right] \tag{4}$$

$$V_3(\Omega) \propto \frac{\omega_0}{c}\left[dx_{C_1}e^{i\Omega L/c} + dx_{D_1}e^{i\Omega L/c} + dx_A e^{2i\Omega L/c} + dx_B\right] \tag{5}$$

$$V_4(\Omega) \propto \frac{\omega_0}{c}\left[dx_{C_1}e^{i\Omega L/c} + dx_{D_1}e^{i\Omega L/c} + dx_A + dx_B e^{2i\Omega L/c}\right] \tag{6}$$

where $dx_{C_1}, dx_{C_2}\cdots$ are the amplitudes of the displacement of C_1, C_2 and so on. Using electric subtracters, we will obtain the DFI signal $V_{\rm DFI}(\omega)$, by combining the signals;

$$V_{\rm DFI}(\Omega) = (V_1(\Omega) - V_2(\Omega)) - (V_3(\Omega) - V_4(\Omega)). \tag{7}$$

As was given by Eq. (16) in [9], when the $\eta - \xi$ polarized GWs come along the z direction, the DFI signal will respond to the GWs in such a way that

$$H_{\rm GW} = \frac{i\omega_0 h e^{i2\Omega L/c}}{4\Omega}\left[(2-\sqrt{2})[1-e^{(4+2\sqrt{2})i\Omega L/c}] + (2+\sqrt{2})[e^{4i\Omega L/c} - e^{2\sqrt{2}i\Omega L/c}]\right]. \tag{8}$$

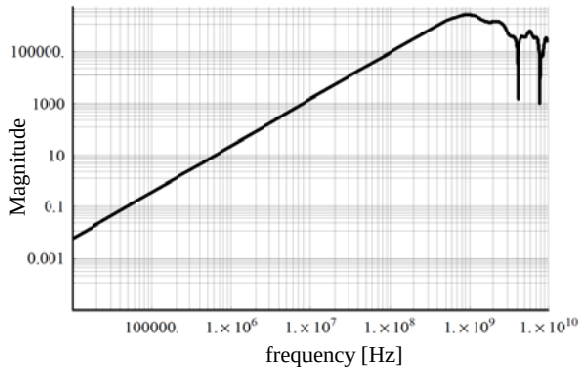

Figure 4. Transfer function from the GW signal to the DFI signal when $L = 0.4$ m. The peak frequency depends on the length L. In our experiment, GW signals are expected around 200 MHz. The GW effects will be simulated by using multiple EOMs.

where we have denoted with h the amplitude of the GW. Figure 4 shows the plot of the response when the arm length L=0.4m. The GW signals retain around approximately 200 MHz for this scale. The frequency of the sensitivity peak depends on L. Below the peak frequency, the response is attenuated in proportional to f^2. It is noted that the DFI technique is not yet known to offer a practical advantages in strain sensitivity at low frequencies for the GW detectors of current sensitivity because there are merely little displacement noises at high frequencies where the GW signals are retained. The observation range can be lower for the DFI with longer arms.

4.1. Optical-displacement simulator

The mirror noises are injected by EOMs in the same way as the previous proof-of-principle experiment shown in [10]. For example, when the displacements of mirror D_2 is simulated, we put an EOM near D_2. The beamsplitter noises will be simulated by two EOMs for one beamsplitter. Although there must be four identical EOMs to mimic the beamsplitter displacements naively, the two EOMs will be applied on the two optical paths because of the fact that actuating two lengths differentially and actuating one length of the two are similar effects. For example, when the displacements of beamsplitter A is simulated, one EOM will be put near A on the AC_2 side, and the other EOM will be put near A on the AD_1 side.

4.2. GW simulator

The GWs affects not only one point on the laser path but the whole path. Therefore putting an EOM on a laser path can not simulate such effects because it yields phase changes at only one point where it is putting on. A straight forward way to simulate the real GW effects is to fill EOMs the whole laser paths. However, such many EOMs covering laser paths will cause the serious reduction of interferometer contrast. Therefore we adopt a tricky procedure. First, we will put an EOM at one point and take data then put the EOM at the next point and take data. Repeating this procedure and summing them, we will be able to duplicate the GW effect on the laser path.

5. Conclusions

In this paper we have presented the demonstration of the partially implemented DFI. The noise suppression of about two orders of magnitude was achieved. The displacement noise of a beamsplitter was injected by the attached PZT. In addition, the next experimental plan has been presented. The DFI in the 3D configuration will be built and operated. The GW-signal survival will be confirmed around 200 MHz while all the optical displacements are canceled in the DFI signals. The optical displacements will be simulated by EOMs.

Acknowledgments
The authors gratefully acknowledge the support of the research Japan Society for the Promotion of Science and Grant-in-Aid for Scientific Research. This research is also supported in part by the United States National Science Foundation grant PHY-0107417 for the construction and operation of the LIGO Laboratory and the Science. This paper has LIGO Document Number LIGO-P070131-00-Z.

References

[1] A. Abramovici *et al.*, Science **256**, 325 (1992)
[2] D. Sigg *et al.*, Class. Quantum Grav. **23**, S51 (2006)
[3] F. Acernese *et al.*, Class. Quantum Grav. **23**, S635 (2006)
[4] H. Lück *et al.*, Class. Quantum Grav. **23**, S71 (2006)
[5] M. Ando *et al.*, Class. Quantum Grav. **22**, S881 (2006)
[6] D. E. McClelland *et al.*, Class. Quantum Grav. **23**, S41 (2006)
[7] S. Kawamura and Y. Chen, 2004 *Phys. Rev. Lett.* **93** 211103
[8] Y. Chen and S. Kawamura, 2006 *Phys. Rev. Lett.* **96** 231102
[9] Y. Chen *et al*, 2006 *Phys. Rev. Lett.* **97** 151103
[10] S. Sato *et al*, 2007 *Phys. Rev. Lett.* **98** 141101
[11] S. Sato *et al*, in this volume